Observation of hourglass nodal lines in photonics

Xia, Lingbo; Guo, Qinghua; Yang, Biao; Han, Jiaguang; Liu, Chao-xing; Zhang, Weili; Zhang, Shuang

DOI:
10.1103/PhysRevLett.122.103903

Editors' Suggestion

Observation of Hourglass Nodal Lines in Photonics

Lingbo Xia,[1,2,*] Qinghua Guo,[1,*] Biao Yang,[1,3,*] Jiaguang Han,[2,†] Chao-Xing Liu,[4,‡] Weili Zhang,[2,5] and Shuang Zhang[1,§]

[1]*School of Physics and Astronomy, University of Birmingham, Birmingham, B15 2TT, United Kingdom*

[2]*Center for Terahertz Waves and College of Precision Instrument and Optoelectronics Engineering, Tianjin University and the Key Laboratory of Optoelectronics Information and Technology (Ministry of Education), Tianjin 300072, China*

[3]*College of Advanced Interdisciplinary Studies, National University of Defense Technology, Changsha 410073, China*

[4]*Department of Physics, Pennsylvania State University, University Park, Pennsylvania 16802-6300, USA*

[5]*School of Electrical and Computer Engineering, Oklahoma State University, Stillwater, Oklahoma 74078, USA*

(Received 18 August 2018; published 15 March 2019)

Nodal line semimetals exhibiting line degeneracies in three-dimensional momentum space have been demonstrated recently. In general, the presence of nodal line semimetals is protected by special symmetries, such as mirror symmetry. However, these symmetries are usually necessary but not sufficient conditions, as nodal lines can be annihilated even without breaking them. Very recently, nodal line semimetal possessing an hourglass-shaped band structure emerges as a more robust candidate, where line degeneracies cannot be annihilated while preserving all underlying spatial symmetries. Here, for the first time, we experimentally demonstrate the presence of an hourglass nodal line (HNL) in photonic metacrystal at microwave frequency. We observe the HNL through near-field scanning of the spatial fields, followed by subsequent Fourier transformations. The observed photonic HNL resides in a clean and large frequency interval and is immune to symmetry preserving perturbation, which provides an ideal robust platform for photonic applications, such as anomalous quantum oscillation, spontaneous emission and resonant scattering.

DOI: 10.1103/PhysRevLett.122.103903

Introduction.—Topological physics has attracted great interest in the past decades [1–4], which usually requires the protection by symmetries, such as time-reversal and mirror symmetries. Depending on whether there is a complete gap between valence and conduction bands, symmetry protected topological phases can be categorized into two classes: those that are gapped or gapless [3]. The gapped nontrivial topological phases include topological insulators and superconductors [5]. Based on the dimension of degeneracies in the momentum space, the gapless topological phases can be sorted as Weyl or Dirac semimetals (0D), nodal line or chain semimetals (1D), and nodal surface semimetals (2D) [4]. The concepts of topological band theory and nontrivial topological phases have been extended from solid-state systems into photonic systems in the last decade. Various topological phenomena have been realized in photonics, such as the photonic quantum Hall effect [6–9], topological insulator [10–15], Weyl or Dirac semimetals [16–26], and nodal lines [27,28]. Among them, Weyl semimetals requiring breaking of either time-reversal or inversion symmetry are robust under general perturbations, as all three Pauli matrices have been involved exhaustively. Nodal line semimetals [27–36] with line degeneracies (1D) only consist two of the anticommuting Pauli matrices; hence extra symmetry constraints are required to make it stable. However, simple point symmetries only provide the orthogonality condition between different modes and cannot robustly guarantee the existence of nodal lines. For example, most nodal line semimetals arise from accidental degeneracy between two bands

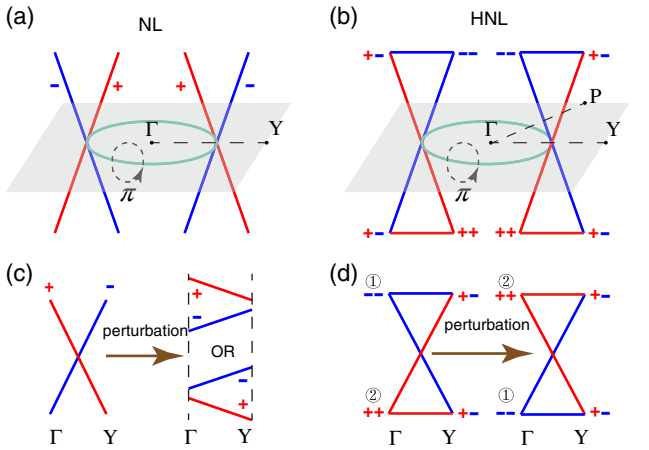

FIG. 1. (a) Nodal lines formed by accidental degeneracy possess opposite eigenvalues of mirror symmetry. (b) HNL formed by an hourglass-shaped band dispersion that goes around a circle in the momentum space. (c) Schematically illustrating that nodal line degeneracy is removed by perturbations. (d) Schematically illustrating the robustness of HNL. Note, the blue and red bands correspond to negative (−1) and positive (+1) eigenvalue of the mirror symmetries. Γ and *Y* denote the BZ center and edge points, respectively.

with opposite mirror eigenvalues, as shown in Fig. 1(a). Such nodal lines can be easily broken or removed from the Brillouin zone (BZ) by certain perturbations, such as structure variation, without breaking any underlying symmetries, as schematically shown in Fig. 1(c).

To overcome the fragileness of the typical nodal line semimetals, an hourglass nodal line (HNL) [37,38] is proposed, which is formed by an hourglass-shaped band dispersion around a loop in the momentum space, as shown in Fig. 1(b). The formation of HNL involves four bands, in contrast to only two bands in previous demonstrations of nodal lines. Figure 1(d) shows its robustness against symmetry preserving perturbations. Even when the double degeneracy points are flipped upside down ($1 \leftrightarrow 2$), the hourglass-shaped zigzag pattern still persists. Thus, HNL provides a robust platform for future applications. Here, we theoretically propose the presence of HNL in a metacrystal at the microwave region and, for the first time, experimentally demonstrate HNL in photonics.

Results.—Theoretical analysis of HNL in photonic metacrystal: For the metacrystal, each unit cell consists of two sets of structures α_1 and α_2, as shown in the left panel of Fig. 2(a), where each set includes two coupled metallic splitting resonant rings. The bottom and top view of the structure is shown in the right panel of Fig. 2(a). In the microwave regime, those metallic components are regarded as perfect electric conductor (PEC). The photonic metacrystal is constructed in a simple tetragonal lattice (lattice periods are $p_x = p_y = 4$ mm, $p_z = 5$ mm) with metallic structures embedded in a hosting material with dielectric

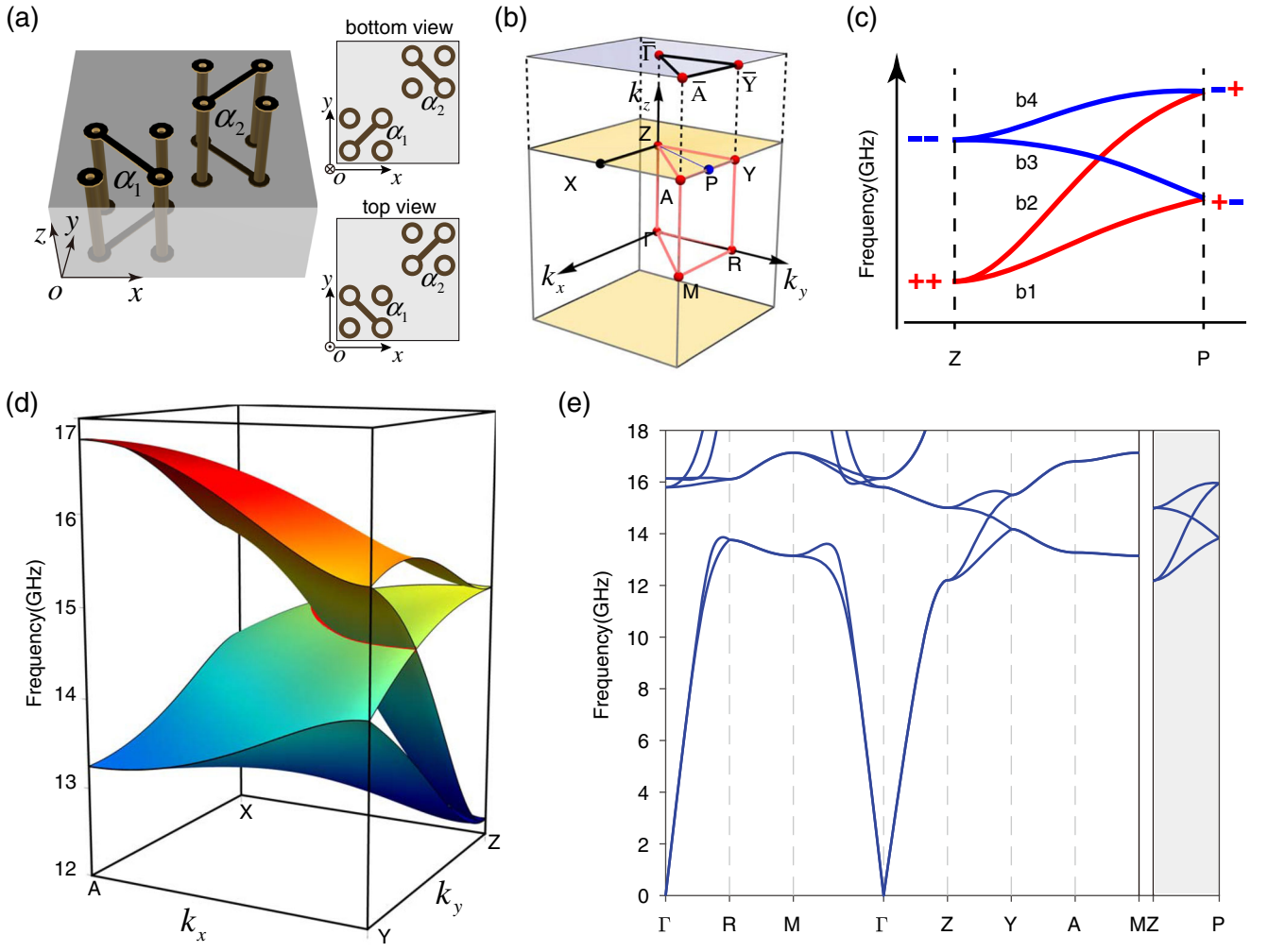

FIG. 2. (a) Unit cell of metallic structure layer with in-plane period $p_x = p_y = 4$ mm and thickness of 2 mm are shown in the left panel. Between two structure layers, there is a spacer layer with thickness of 3 mm. The bottom or top view of the metallic layer is given in the right panel. (b) The first (bulk) BZ of tetragonal lattice with reduced (bulk) BZ boxed by red triangle prism. The $k_z = \pi/p_z$ plane is highlighted in yellow, where HNL exists. The upper blue plane shows the surface BZ. (c) The hourglass-shaped dispersion along line Z-P as indicated in (b). The red and blue lines are bands corresponding to glide mirror ($\tilde{M}_z$) eigenvalue of $+1$ and -1, respectively. $b1 - b4$ are four bands forming an hourglass-shaped dispersion. (d) The quarter view of photonic HNL dispersion on $k_z = \pi/p_z$ plane. The HNL degeneracy is plotted in red. (e) The bulk bands dispersion along high symmetry lines.

constant of 2.2. The lattice possesses nonsymmorphic space group $P4/nbm$ (No. 125), which includes three glide mirror operations involving half lattice translation, $\tilde{M}_x: (x,y,z) \to (-x, y+\frac{1}{2}, z)$, $\tilde{M}_y: (x,y,z) \to (x+\frac{1}{2}, -y, z)$, and $\tilde{M}_z: (x,y,z) \to (x+\frac{1}{2}, y+\frac{1}{2}, -z)$. The tilde above the mirror operation symbol indicates that it is a nonsymmorphic symmetry operator. These are crucial in our analysis. Figure 2(b) shows the tetragonal BZ and surface BZ with the reduced BZ boxed by red lines and high symmetry points highlighted by red spheres. In this Letter, the theoretical results are calculated by the "Eigenmode Solver" module of CST MICROWAVE STUDIO (see Supplemental Material [39]).

The photonic HNL is located on the $k_z = \pi/p_z$ plane (Z-A-Y plane) highlighted in yellow in Fig. 2(b). The bands located on the BZ boundaries of the $k_z = \pi/p_z$ plane (e.g., the line X-A-Y) are all doubly degenerate due to the anticommutation relation between $\tilde{M}_z$ and $\tilde{M}_y$ (or $\tilde{M}_x$). Considering an arbitrary point P located on the A-Y line as an example, the combination of $\tilde{M}_z$ and $\tilde{M}_y$ yields

$$\begin{aligned} \tilde{M}_z\tilde{M}_y:\ (x,y,z) &\to \left(x+1, -y+\tfrac{1}{2}, -z\right), \\ \tilde{M}_y\tilde{M}_z:\ (x,y,z) &\to \left(x+1, -y-\tfrac{1}{2}, -z\right). \end{aligned} \tag{1}$$

Let $|\varphi\rangle$ be an arbitrary common eigenstate of the $\tilde{M}_z$ operator and the Hamiltonian at P point. We have $\tilde{M}_y\tilde{M}_z|\varphi\rangle = e^{ik_xp_x}e^{-ik_yp_y/2}C_{2x}|\varphi\rangle$ and $\tilde{M}_z\tilde{M}_y|\varphi\rangle = e^{ik_yp_y}(e^{ik_xp_x}e^{-ik_yp_y/2}C_{2x}|\varphi\rangle)$, where C_{2x} is twofold rotation about the x axis. Since $k_y = \pi/p_y$ at the P point, we obtain $\tilde{M}_z\tilde{M}_y|\varphi\rangle = -\tilde{M}_y\tilde{M}_z|\varphi\rangle$. Thus, we obtain the anticommutation relation [40] between $\tilde{M}_z$ and $\tilde{M}_y$,

$$\{\tilde{M}_y, \tilde{M}_z\} = 0. \tag{2}$$

As $|\varphi\rangle$ is an eigenstate of $\tilde{M}_z$, we have $\tilde{M}_z|\varphi\rangle = \xi|\varphi\rangle$, where $\xi = 1$ (or -1) is the eigenvalue of $\tilde{M}_z$. Then $\tilde{M}_z\tilde{M}_y|\varphi\rangle = -\xi\tilde{M}_y|\varphi\rangle$. Because of the anticommutation in Eq. (2), one obtains

$$\langle\varphi|\tilde{M}_y|\varphi\rangle = \langle\varphi|\tilde{M}_z^{-1}\tilde{M}_z\tilde{M}_y|\varphi\rangle = -\langle\varphi|\tilde{M}_y|\varphi\rangle, \tag{3}$$

ensuring the orthogonality between $|\varphi\rangle$ and $\tilde{M}_y|\varphi\rangle$. Both states $|\varphi\rangle$ and $\tilde{M}_y|\varphi\rangle$ are eigenstates of the Hamiltonian and possess opposite eigenvalues of the operator $\tilde{M}_z$. The two states $|\varphi\rangle$ and $\tilde{M}_y|\varphi\rangle$ are degenerate due to orthogonality, leading to the conclusion that all the eigenstates are doubly degenerate at any arbitrary point on A-Y line.

Next, we show that the double degeneracy at the Z point is protected by higher irreducible representations of D_{4h}. As we know, each unit cell contains two sets α_1 and α_2. Each set includes two perpendicularly positioned splitting resonant rings. For the wave propagating along the z direction at low frequency, there exists a pair of hybrid modes arising from the in-phase and out-phase coupling between α_1 and α_2. In addition, due to the C_4 symmetry ($\pi/2$ rotation about the z axis) of the crystal, there exists another pair of in-phase and out-phase coupled hybrid modes, which is related to the former pair of modes by a C_4 rotation. Therefore, there must exist a pair of degenerate modes due to the in-phase coupling between the two set α_1 and α_2, and another pair of degenerate modes originating from the out-phase coupling (see Supplemental Material [39]). More mathematically, the little group (or wave vector group) at the Z point is D_{4h} (or $4/mmm$ in Hermann-Mauguin notation). The two pairs of degenerate frequencies due to the in-phase and out-phase coupling belong to higher irreducible representations E_u and E_g, which possess $\tilde{M}_z$ eigenvalue 1 and -1, respectively. Finally, an hourglass-shaped band dispersion will be formed as the four bands travel from the Z point to an arbitrary point P on the A-Y line. $\tilde{M}_z$ symmetry exists for the whole $k_z = \pi/p_z$ plane, and thus any states on this plane can be labeled by the eigenvalue of $\tilde{M}_z$ [blue or red lines in Figs. 1(b), 1(d), and 2(c)]. Since the two degenerate bands possess the same eigenvalue of $\tilde{M}_z$ at the Z point and opposite eigenvalues at point P, there must exist a pair switching along the Z-P line, and the two crossing bands must possess opposite eigenvalues, thus leading to an hourglass-shaped band dispersion, as shown in Fig. 2(c). As P point can freely move along the BZ boundaries on the $k_z = \pi/p_z$ plane (e.g., X-A-Y line), an hourglass ring naturally shows up, which ensures the appearance of HNL. A quarter view of the HNL is given in Fig. 2(d). The nodal degeneracy is highlighted by the red line. The band structure along the high symmetry lines is plotted in Fig. 2(e), from which one can see a nearly ideal photonic HNL located in a quite broad and clean frequency range with the frequency variation ($\Delta\omega/\omega_{\text{middle}}$) less than 1%.

Experimental observation of photonic HNL.—The sample is fabricated by the standard printed circuit board (PCB) technique. Figure 3(a) shows the top view of the structure layer with a thickness of 2 mm. In addition, a 3-mm-thick spacer layer, made of dielectric material (F4BM) with the relative permittivity of 2.2, is placed between the adjacent copper-clad PCBs to prevent short contacting from metallic wires. Each layer of the PCB sample has 100×100 unit cells. By stacking the PCB sample layer by layer along the z direction (nine unit cells), we construct a photonic metacrystal in the microwave band. Near-field scanning is carried out to map the HNL bulk band dispersion. In our experimental configuration, one z-oriented electrical dipole antenna acting as a source is positioned at the side of the sample [as shown in Fig. 3(b)]. Another z-oriented electrical dipole antenna serving as probe raster scans the top surface of the sample. The distance between the probe antenna and the top surface is around 1 mm, ensuring the

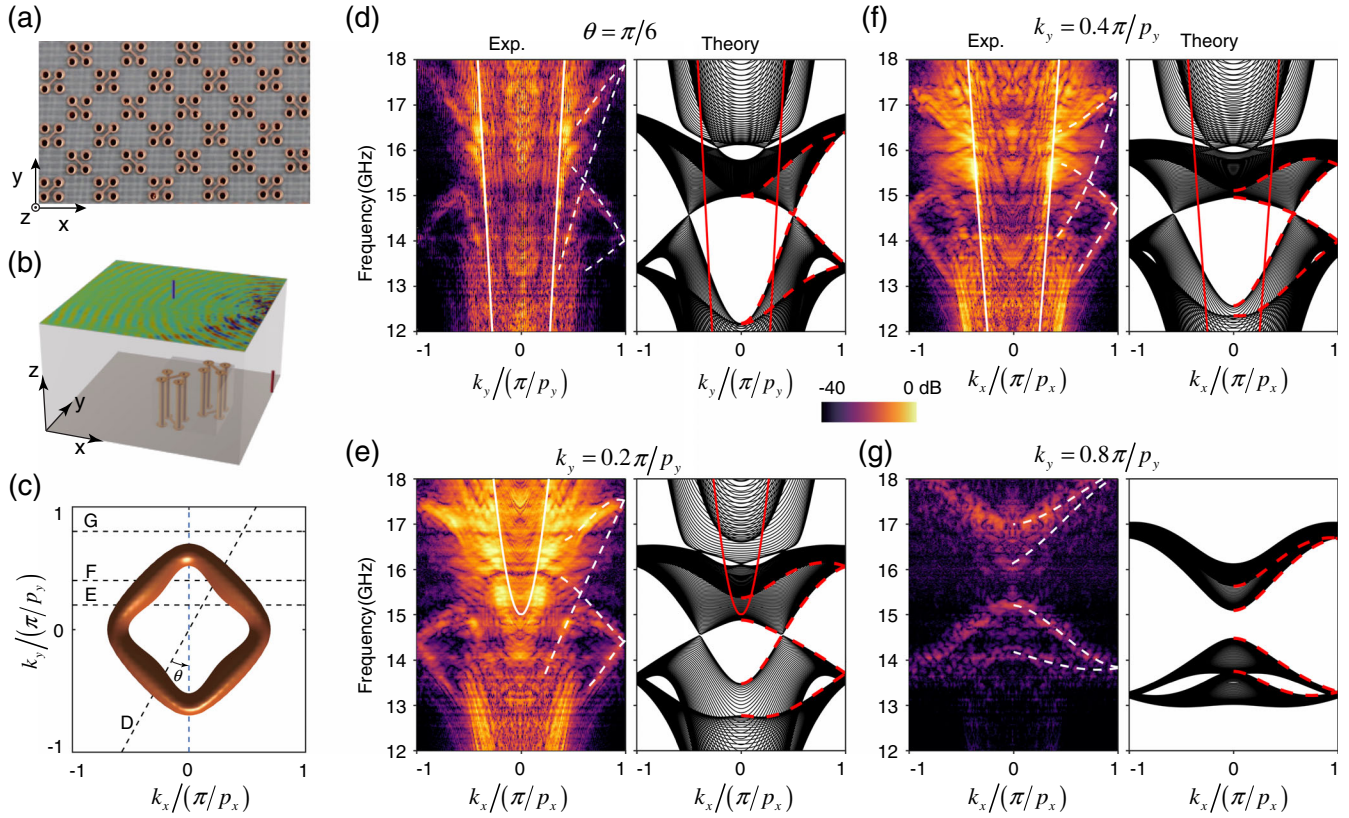

FIG. 3. (a) Photograph of top surface of the sample fabricated by printed circuit board technology. (b) Experiment setup configuration with source denoted by red cylinder and probe denoted by blue cylinder, respectively. The top surface illustrates the real part of electric field E_z at frequency of 14.8 GHz. (Inset) Structure unit cell. (c) The theoretical equifrequency contour at 14.8 GHz near the HNL, which is shaped in torus. The four dashed lines $k_x = k_y \tan\theta$, $k_y = 0.2\pi/p_y$, $k_y = 0.4\pi/p_y$, and $k_y = 0.8\pi/p_y$ labeled by D–G in the surface BZ correspond to four cases (d)–(g), respectively. (d) The experiment (left) and theoretical (right) band projection when $\theta = \pi/6$. (e)–(g) The experiment (left) and theoretical (right) band projection along $k_y = 0.2\pi/p_y$, $0.4\pi/p_y$, and $0.8\pi/p_y$ line, respectively. The two lines $k_y = 0.2\pi/p_y$ and $0.4\pi/p_y$ intersect with the HNL. The $k_y = 0.8\pi/p_y$ line locates outside the HNL. Note that in Figs. 3(d)–(3g), the white line (left) and red line (right) denote the light cone. The white dashed lines in the left panel illustrate hourglass-shaped band dispersion. In the right panel, the red dashed lines show hourglass-shaped band dispersion simulated on $k_z = \pi/p_z$.

sensitive detection of evanescent tails of the bulk states. Both the source and probe electrical dipoles are connected to a vector network analyzer (VNA: Keysight-N5234B, 10 MHz–43.5 GHz), which can measure both the amplitude and phase of the electromagnetic field simultaneously in a broad frequency range. Figure 3(b) gives the experiment setup, with source and probe denoted by red and blue cylinders, respectively. Its top surface illustrates the real part of E_z at a frequency of 14.8 GHz. By performing subsequent Fourier transformation upon the detected spatial fields, we obtain the projected equifrequency contours (EFCs) containing a series of discretized k_z values on the surface BZ. The torus in Fig. 3(c) shows the theoretical bulk EFC at 14.8 GHz. Four lines $k_x = k_y \tan\theta$, $k_y = 0.2\pi/p_y$, $k_y = 0.4\pi/p_y$, and $k_y = 0.8\pi/p_y$ on the surface BZ are denoted by D, E, F, and G, respectively. They correspond to four cases in Figs. 3(d)–3(g). The left and right panels in Fig. 3(d) show the experimentally measured and theoretical simulated band spectrum along the line $k_x = k_y \tan(\pi/6)$ in the surface BZ, respectively. The white (left panel) and red (right panel) lines denote the light cone. Although the modes from crystals inside the light cone cannot be easily distinguished due to mixed projected bulk bands in air medium, the hourglass-shaped bands denoted by the white dashed lines located outside the light cone can be clearly recognized. The red dashed line in the theoretical panel denotes the hourglass-shaped bulk bands on the $k_z = \pi/p_z$ plane. Clearly, the density of states vanishes around the hourglass node. Similarly, the left and right panels in Figs. 3(e)–3(g) illustrate the experimentally measured and theoretical simulated band spectra along the lines of $k_y = 0.2\pi/p_y$, $0.4\pi/p_y$, and $0.8\pi/p_y$, respectively. The $k_y = 0.2\pi/p_y$ and $0.4\pi/p_y$ lines in the surface BZ intersect with the HNL, showing linear crossings in their dispersions. On the other hand, the $k_y = 0.8\pi/p_y$ line is located outside the HNL, exhibiting a band gap in the spectrum.

The experimentally measured EFCs in momentum space at 14.8, 15.16, and 15.65 GHz, which correspond to

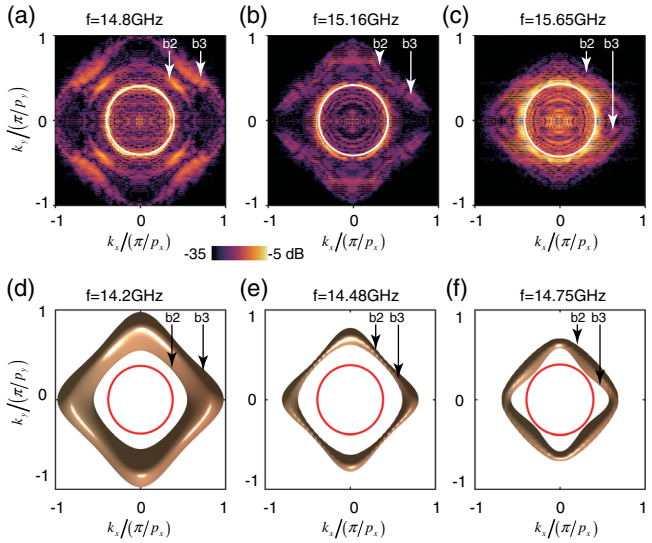

FIG. 4. (a)–(c) The experimental results of projected E_z field at frequency of 14.8, 15.16, and 15.65 GHz, respectively. The positions of the second band ($b2$) and third band ($b3$) are pointed out by white arrows, where $b2$ and $b3$ are hourglass-shaped bands as denoted in Fig. 2(c). The white circles denote the light cone. (d)–(f) The theoretical results of EFCs at frequency of 14.2, 14.48, and 14.75 GHz, respectively. The red circles denote the light cone.

frequencies below, approaching, and above the experimental HNL, are shown in Figs. 4(a)–4(c), respectively. The positions of the second band ($b2$) and third band ($b3$) are indicated by white arrows, where $b2$ and $b3$ are two relevant bands forming HNL as shown in Fig. 2(c). The circle in the center denoted by the white line indicates the light cone. The two EFCs at 14.8 GHz located far away from the light cone are easily distinguished. At a frequency of 15.16 GHz, the two EFCs nearly merge into each other. The third band at a frequency of 15.65 GHz is very close to the light cone, which makes it hard to distinguish. The theoretical simulated EFCs at the frequencies of 14.2, 14.45, and 14.75 GHz, which correspond to frequencies below, approaching, and above the theoretical HNL, are illustrated in Figs. 4(d)–4(f), respectively. Comparing with the experimental results in Figs. 3 and 4, the theoretical results show a strong resemblance to the experimental ones except for a small frequency shift due to fabrication inaccuracy.

To summarize, we theoretically propose HNL in a carefully designed photonic metacrystal, which is protected by glide mirror symmetry and high irreducible representation of D_{4h}. The glide mirror involving fractional lattice translation causes the anticommutation relation [Eq. (2)] and then result in double degeneracy at the BZ edge, which is crucial to the realization of HNL. By performing near-field scanning in the microwave region, for the first time, we experimentally observed the HNL in a photonic metacrystal structure, which provides a powerful platform for studying topological phases. Also, the HNL can support negative refraction [41], which usually requires simultaneously well-designed negative effective permittivity and permeability in the overlapped frequency range. Other photonic applications that arise from the unique density of states of the nodal line include blackbody radiation [42], spontaneous emission, and resonant scattering [43]. With the introduction of a pseudomagnetic field (synthetic vector potential), anomalous quantum oscillation may also be observed in the HNL [44].

We acknowledge the support from ERC Consolidator Grant (TOPOLOGICAL), Horizon 2020 Action (Project No. 734578), National Natural Science Foundation of China (Grant No. 11604216) and the Chinese Scholarship Council Grant No. 201606250059, (L. X.). C. X. L. acknowledges the support from Office of Naval Research (Grant No. N00014-15-1-2675).

*These authors contributed equally to this work.
†Corresponding author.
jiaghan@tju.edu.cn
‡Corresponding author.
cxl56@psu.edu
§Corresponding author.
s.zhang@bham.ac.uk

[1] M. Z. Hasan and C. L. Kane, Rev. Mod. Phys. **82**, 3045 (2010).
[2] X.-L. Qi and S.-C. Zhang, Rev. Mod. Phys. **83**, 1057 (2011).
[3] C.-K. Chiu, J. C. Y. Teo, A. P. Schnyder, and S. Ryu, Rev. Mod. Phys. **88**, 035005 (2016).
[4] N. P. Armitage, E. J. Mele, and A. Vishwanath, Rev. Mod. Phys. **90**, 015001 (2018).
[5] A. P. Schnyder, S. Ryu, A. Furusaki, and A. W. W. Ludwig, Phys. Rev. B **78**, 195125 (2008).
[6] F. D. M. Haldane and S. Raghu, Phys. Rev. Lett. **100**, 013904 (2008).
[7] Z. Wang, Y. Chong, J. D. Joannopoulos, and M. Soljačić, Nature (London) **461**, 772 (2009).
[8] Y. Poo, R.-x. Wu, Z. Lin, Y. Yang, and C. T. Chan, Phys. Rev. Lett. **106**, 093903 (2011).
[9] K. Fang, Z. Yu, and S. Fan, Nat. Photonics **6**, 782 (2012).
[10] A. B. Khanikaev, S. Hossein Mousavi, W.-K. Tse, M. Kargarian, A. H. MacDonald, and G. Shvets, Nat. Mater. **12**, 233 (2013).
[11] M. C. Rechtsman, J. M. Zeuner, Y. Plotnik, Y. Lumer, D. Podolsky, F. Dreisow, S. Nolte, M. Segev, and A. Szameit, Nature (London) **496**, 196 (2013).
[12] W.-J. Chen, S.-J. Jiang, X.-D. Chen, B. Zhu, L. Zhou, J.-W. Dong, and C. T. Chan, Nat. Commun. **5**, 5782 (2014).
[13] L.-H. Wu and X. Hu, Phys. Rev. Lett. **114**, 223901 (2015).
[14] A. Slobozhanyuk, S. H. Mousavi, X. Ni, D. Smirnova, Y. S. Kivshar, and A. B. Khanikaev, Nat. Photonics **11**, 130 (2017).
[15] Y. Yang, Z. Gao, H. Xue, L. Zhang, M. He, Z. Yang, R. Singh, Y. Chong, B. Zhang, and H. Chen, arXiv:1804.03595.
[16] L. Lu, L. Fu, J. D. Joannopoulos, and M. Soljačić, Nat. Photonics **7**, 294 (2013).

[17] L. Lu, Z. Wang, D. Ye, L. Ran, L. Fu, J. D. Joannopoulos, and M. Soljačić, Science **349**, 622 (2015).
[18] W.-J. Chen, M. Xiao, and C. T. Chan, Nat. Commun. **7**, 13038 (2016).
[19] M. Xiao, Q. Lin, and S. Fan, Phys. Rev. Lett. **117**, 057401 (2016).
[20] Q. Lin, M. Xiao, L. Yuan, and S. Fan, Nat. Commun. **7**, 13731 (2016).
[21] W. Gao, B. Yang, M. Lawrence, F. Fang, B. Béri, and S. Zhang, Nat. Commun. **7**, 12435 (2016).
[22] J. Noh, S. Huang, D. Leykam, Y. D. Chong, K. P. Chen, and M. C. Rechtsman, Nat. Phys. **13**, 611 (2017).
[23] Q. Guo, B. Yang, L. Xia, W. Gao, H. Liu, J. Chen, Y. Xiang, and S. Zhang, Phys. Rev. Lett. **119**, 213901 (2017).
[24] Q. Wang, M. Xiao, H. Liu, S. Zhu, and C. T. Chan, Phys. Rev. X **7**, 031032 (2017).
[25] L. Xia, W. Gao, B. Yang, Q. Guo, H. Liu, J. Han, W. Zhang, and S. Zhang, Laser Photonics Rev. **12**, 1700226 (2018).
[26] B. Yang, Q. Guo, B. Tremain, R. Liu, L. E. Barr, Q. Yan, W. Gao, H. Liu, Y. Xiang, J. Chen, C. Fang, A. Hibbins, L. Lu, and S. Zhang, Science **359**, 1013 (2018).
[27] Q. Yan, R. Liu, Z. Yan, B. Liu, H. Chen, Z. Wang, and L. Lu, Nat. Phys. **14**, 461 (2018).
[28] W. Gao, B. Yang, B. Tremain, H. Liu, Q. Guo, L. Xia, A. P. Hibbins, and S. Zhang, Nat. Commun. **9**, 950 (2018).
[29] Y. Kim, B. J. Wieder, C. L. Kane, and A. M. Rappe, Phys. Rev. Lett. **115**, 036806 (2015).
[30] F. Chen, W. Hongming, D. Xi, and F. Zhong, Chin. Phys. B **25**, 117106 (2016).
[31] T. Bzdušek, Q. Wu, A. Rüegg, M. Sigrist, and A. A. Soluyanov, Nature (London) **538**, 75 (2016).
[32] G. Bian *et al.*, Nat. Commun. **7**, 10556 (2016).
[33] J. He, X. Kong, W. Wang, and S.-P. Kou, arXiv:1709.08287.
[34] M. Hirayama, R. Okugawa, T. Miyake, and S. Murakami, Nat. Commun. **8**, 14022 (2017).
[35] T. Kawakami and X. Hu, Phys. Rev. B **96**, 235307 (2017).
[36] R. Okugawa and S. Murakami, Phys. Rev. B **96**, 115201 (2017).
[37] R. Takahashi, M. Hirayama, and S. Murakami, Phys. Rev. B **96**, 155206 (2017).
[38] B. Fu, X. Fan, D. Ma, C.-C. Liu, and Y. Yao, Phys. Rev. B **98**, 075146 (2018).
[39] See Supplemental Material at http://link.aps.org/supplemental/10.1103/PhysRevLett.122.103903 for the symmetry analysis along $\Gamma - Z$ line, simulation description with CST Microwave Studio, resonant property of the structure and verification of the robustness of the HNL.
[40] X.-Y. Dong and C.-X. Liu, Phys. Rev. B **93**, 045429 (2016).
[41] L. Wang, S.-K. Jian, and H. Yao, Phys. Rev. A **93**, 061801 (2016).
[42] P. J. Roberts, in *IEE Colloquium on Semiconductor Optical Microcavity Devices and Photonic Bandgaps* (IEEE Xplore, 1996), paper 1996/267, p. 4/1.
[43] M. Zhou, L. Ying, L. Lu, L. Shi, J. Zi, and Z. Yu, Nat. Commun. **8**, 1388 (2017).
[44] H. Yang, R. Moessner, and L.-K. Lim, Phys. Rev. B **97**, 165118 (2018).